



CrossMark  
 click for updates

Cite this: *RSC Adv.*, 2015, 5, 97272

## Tailored synthesis of $\text{CoO}_x$ thin films for catalytic application†

Shi-Bin Fan,<sup>ab</sup> Guan-Fu Pan,<sup>ab</sup> Jing Liang<sup>a</sup> and Zhen-Yu Tian<sup>\*a</sup>

Cobalt oxide thin films were systematically synthesized on an inert carrier by pulsed-spray evaporation chemical vapor deposition (PSE-CVD). The effect of substrate temperature on the structure, morphology and surface composition of the prepared films was investigated by XRD, FTIR, SEM and XPS spectroscopies. An *in situ* diffuse reflectance infrared Fourier transform spectroscopy (*in situ* DRIFTS) and a gas chromatograph (GC) were involved to identify the surface and gaseous species occurring in the total oxidation of propene as a representative of VOCs, respectively. The structural analysis indicated that the obtained thin films transformed from CoO to pure  $\text{Co}_3\text{O}_4$  spinel as the temperature rose from 350 to 450 °C. A homogeneous grain distribution was observed. For all samples, oxygen was mainly composed of lattice oxygen and adsorbed oxygen constituted a minor proportion. The catalytic tests showed that all the thin films exhibited competitive performances to those of noble metals. According to the observed adsorption peaks of propene at low-temperature and transformation of CoO– $\text{Co}_3\text{O}_4$  from the *in situ* DRIFTS spectra, a combined redox and L–H mechanism was proposed for the catalytic oxidation of propene over cobalt oxide films. The porous structure and adsorbed oxygen on the film surface may well contribute to the catalytic oxidation of propene.

Received 28th September 2015

Accepted 3rd November 2015

DOI: 10.1039/c5ra20013j

[www.rsc.org/advances](http://www.rsc.org/advances)

## Introduction

Volatile organic compounds (VOCs) are one of the main air pollutants originating mainly from transportation and the combustion of different fuels.<sup>1–3</sup> Due to their toxicity to human health<sup>4</sup> and involvement in the formation of photochemical smog,<sup>5</sup> many countries have imposed strict standards to reduce the industrial VOCs emissions. Several methods have been used in the past few decades, such as thermal incineration,<sup>6</sup> biodegradation,<sup>7</sup> high-energy electron beam treatment,<sup>8</sup> adsorption<sup>9</sup> and absorption.<sup>10</sup> Recently, catalytic oxidation has attracted much attention as one of the most promising VOCs abatement technologies regarding its high efficiency and selectivity to  $\text{CO}_2$ .<sup>11–14</sup> Among the reported catalysts, transition metal oxides (TMOs) exhibit great potential due to its low cost and efficiency compared to the traditional noble metal catalysts.<sup>15,16</sup> Specifically, cobalt oxides ( $\text{CoO}_x$ ) show interesting catalytic properties for the deep oxidation of VOCs. A lot of works have been contributed to the synthesis, characterization and catalytic application of  $\text{Co}_3\text{O}_4$ <sup>17–19</sup> and cobalt-based oxides.<sup>20–23</sup> However, besides  $\text{Co}_3\text{O}_4$

spinel, other cobalt oxides which contain low-valence cobalt are also expected to have promising catalytic activity. Although there are some works focusing on the preparation of individual  $\text{Co}_3\text{O}_4$ <sup>18,24–27</sup> or  $\text{CoO}$ <sup>28,29</sup> available, the systematic and controllable synthesis of  $\text{CoO}_x$  by a direct method for catalytic applications still remains a challenging task. Moreover, in many of the above-mentioned studies,<sup>18,27,28</sup> the substrates or supports generally play significant roles, which prevents the real evaluation of the catalytic performance of  $\text{CoO}_x$ . Thus, it is desired to prepare  $\text{CoO}_x$  on inert substrates.

$\text{CoO}_x$  can be synthesized through several methods, including pulsed laser deposition ( $\text{Co}_3\text{O}_4$ ),<sup>18</sup> sol-gel ( $\text{Co}_3\text{O}_4$ ),<sup>24</sup> spray pyrolysis ( $\text{Co}_3\text{O}_4$ ),<sup>25,27</sup> sputtering ( $\text{Co}_3\text{O}_4$ ),<sup>26</sup> electrodeposition ( $\text{CoO}$ ),<sup>28</sup> hydrolysis ( $\text{CoO}$ ),<sup>29</sup> solvothermal ( $\text{Co}_3\text{O}_4$  and  $\text{CoO}$ )<sup>30</sup> and excess impregnation ( $\text{Co}_x\text{O}_y$ ).<sup>31</sup> However, with these methods, the purity of the acquired samples was usually difficult to ensure and some of them involved strict conditions or complex treatments. Compared to the above-mentioned techniques, pulsed-spray evaporation chemical vapor deposition (PSE-CVD) is easy to control the quality and thickness of the films on flexible substrates with low cost. In recent years, PSE-CVD has been applied widely to the synthesis of TMOs, such as  $\text{Co}_3\text{O}_4$ ,<sup>32</sup>  $\text{Mn}_3\text{O}_4$ ,<sup>33</sup>  $\text{Co}_{3-x}\text{Fe}_x\text{O}_4$ <sup>34</sup> and  $\text{Co}_{3-x}\text{Cr}_x\text{O}_4$ .<sup>35</sup> It should be mentioned that as a flexible substrate the stainless steel gird mesh is proved to have no or negligible catalytic effect and can be used for most reactors shapes. Thus, PSE-CVD exhibits great potential to prepare  $\text{CoO}_x$  thin films on stainless steel gird mesh for real evaluation of the catalytic performance of  $\text{CoO}_x$  samples.

<sup>a</sup>Institute of Engineering Thermophysics, Chinese Academy of Sciences, 11 Beisihuanxi Road, Beijing 100190, China. E-mail: tianzhenyu@iet.cn; Fax: +86 10 82543184; Tel: +86 10 82543184

<sup>b</sup>University of Chinese Academy of Sciences, Beijing 100049, China

† Electronic supplementary information (ESI) available: Experimental conditions; results of repeated catalytic tests with coated mesh, NCM and a blank system; standard IR spectrum for  $\text{C}_3\text{H}_6$ ; *in situ* DRIFTS spectra for Mesh 350 and 450. See DOI: 10.1039/c5ra20013j

The present work is oriented to synthesize the thin films of  $\text{CoO}_x$  by PSE-CVD in a tailored way. The effect of substrate temperature on the phases of the films was investigated. Several dedicated techniques were used to characterize the prepared films with respect to structure, chemical composition and morphological properties. The catalytic performance of the grown  $\text{CoO}_x$  was investigated for the total oxidation of propene as a representative of VOCs in a fixed-bed quartz reactor. Furthermore, to get an insight into the catalytic mechanism, a newly developed *in situ* diffuse reflectance infrared Fourier transform spectroscopy (DRIFTS) was employed. With this setup, surface adsorbed species can be detected during the catalytic test which provides information to understand the catalytic mechanism.

## Results and discussion

### Structure

The XRD patterns of the  $\text{CoO}_x$  thin films prepared at temperature range of 350–450 °C are displayed in Fig. 1. With the substrate temperature increasing from 350 to 450 °C, the obtained oxide transformed from CoO to pure  $\text{Co}_3\text{O}_4$  gradually. For Mesh 350, peaks at 36.50°, 42.40°, 61.52° and 73.70° can be seen clearly, which are attributed to (111), (200), (220) and (311) orientations of CoO (JCPDS no. 43-1004), respectively. For Mesh 450, well-defined diffraction peaks are observed at  $2\theta$  of 19.00°, 31.27°, 36.85°, 38.54°, 44.81°, 55.66°, 59.36° and 65.24°, which correspond to (111), (220), (311), (222), (400), (422), (511) and (440) orientations of  $\text{Co}_3\text{O}_4$  (JCPDS no. 42-1467). No characteristic peaks of any other impurities were observed with Mesh 450, revealing the high purity of the synthesized thin films. For Mesh 400, both the peaks of CoO and  $\text{Co}_3\text{O}_4$  were observed, which indicates the formation of a mixture of CoO and  $\text{Co}_3\text{O}_4$  spinel. Though weak peaks at 31.27° and 65.24° can also be observed for Mesh 350, the three main peaks manifest that the main composition of Mesh 350 is CoO. The crystallite sizes of the  $\text{CoO}_x$  oxides were estimated to be  $20 \pm 5$  nm by applying Scherrer's formula  $D = 0.89\lambda/\beta \cos \theta$  to the most intense diffraction peak, where  $\lambda = 0.154056$  nm and where  $\beta$  and  $\theta$  represent the full width at half maximum (FWHM) and diffraction angle of the observed peak, respectively.<sup>20</sup>

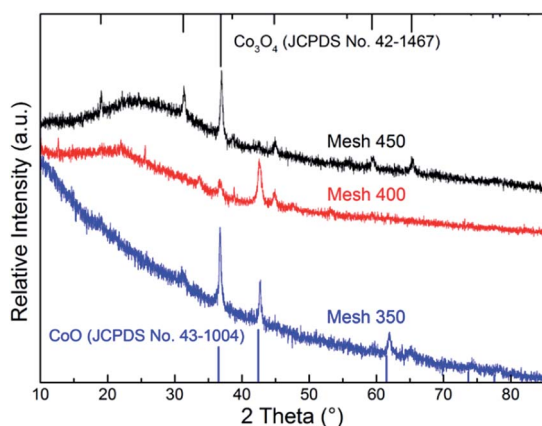


Fig. 1 XRD patterns of the  $\text{CoO}_x$  thin films.

In 2010, Heli and Yadegari reported the CoO preparation by using electrodeposition method.<sup>28</sup> Before deposition, their electrode needed special pretreatments such as polishing and sonication, and all solutions were prepared by doubly distilled water. However, their XRD results are too ambiguous to indicate the formation of pure CoO with good crystallization. Also, a large grain size (800 nm) was reported. Recently, Edla *et al.*<sup>18</sup> synthesized  $\text{Co}_3\text{O}_4$  nanoparticles (NPs) by pulsed laser deposition. These NPs needed heating in Ar atmosphere to remove possible moisture adsorption before CO oxidation tests. The sizes of  $\text{Co}_3\text{O}_4$  NPs were in the range of 18–500 nm which increased with the increasing laser fluence. These reported large grain sizes are expected to offer less surface area and thus lead to limited catalytic activity.

Further analysis with FTIR spectroscopy also confirmed the transformation of the phases from CoO to pure  $\text{Co}_3\text{O}_4$  spinel. As presented in Fig. 2, two obvious bands with maxima at about 657 and 553  $\text{cm}^{-1}$  can be observed and become stronger from Mesh 350 to Mesh 450. It should be noted that there is a strong peak at 580  $\text{cm}^{-1}$  for Mesh 350, while such peak becomes weak for Mesh 400 and can be hardly recognized for Mesh 450 in view of relative intensity. According to the literature,<sup>36,37</sup> the absorption peaks at 553 and 657  $\text{cm}^{-1}$  are assigned to the transversal optical mode (TO) of  $\text{Co}_3\text{O}_4$  and the peak at 580  $\text{cm}^{-1}$  is due to the longitudinal optical mode (LO) of CoO. Therefore, from Fig. 2, it can be deduced that a pure  $\text{Co}_3\text{O}_4$  was acquired at 450 °C and the sample prepared at 400 °C was a mixture of CoO and  $\text{Co}_3\text{O}_4$ , as for Mesh 350, CoO was the main composition synthesized at this temperature. Since exposure to the atmosphere, there are more  $\text{Co}^{3+}$  on the surface than the bulk average which will strengthen  $\text{Co}_3\text{O}_4$  peaks in FTIR. So stronger peaks of  $\text{Co}_3\text{O}_4$  were observed in Fig. 2 for Mesh 350 than Fig. 1.

### Morphology

To have an insight into the surface morphology and spatial organization of the obtained  $\text{CoO}_x$  thin films, SEM was employed here. As displayed in Fig. 3, the morphology of the

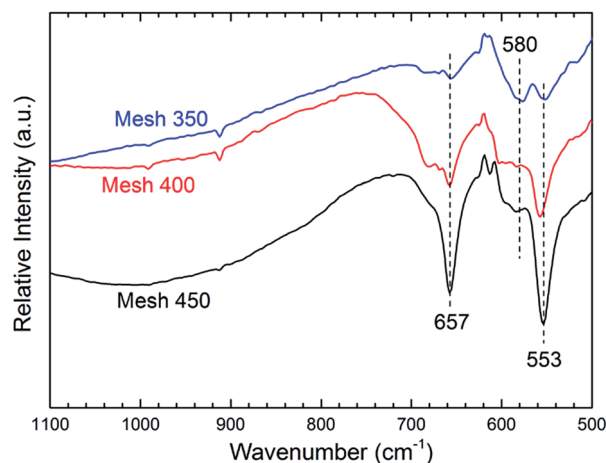


Fig. 2 Effect of the substrate temperature on the diffuse reflectance FTIR spectra of the prepared samples.

deposited thin films could also differ with substrate temperatures. For the sample prepared at 350 °C (Fig. 3a), highly dispersed tiny rods are distributed in the smooth amorphous oxide matrix, which is the highly agglomeration of these rods. Fig. 3b shows a loose spatial organization and a blocky structure with amount of tiny folds. Especially, In fact, beneath these large grains appeared at the surface, agglomeration of smaller structures can also be recognized. Since the grain sizes calculated by XRD data are smaller, it can be deduced that these large grains maybe supported by numerous tiny structures. As for the  $\text{Co}_3\text{O}_4$  spinel obtained at 450 °C (Fig. 3c), numerous small grains with general agglomeration were observed. The micro-morphology can be explained by the growth process which contains nucleation, growth and coalescence process. For the initial grown grains, they could get a bigger size by further deposition and get close to each other. Then, by the coalescence of small ones the larger grains would appear. This agglomeration phenomenon was also observed in the pulsed laser deposition of  $\text{Co}_3\text{O}_4$ .<sup>18</sup> From the three micrographs in Fig. 3, nano-structured particles were observed, which could be due to the agglomeration phenomenon. The size of these particles on the surface seems to be 30–40 nm on average, a little bigger than the values calculated by the XRD analysis. Barreca *et al.*<sup>38</sup> had employed cold-wall low-pressure CVD to prepare  $\text{CoO}_x$  previously, but the substrate needed sputtering as pretreatment. Rounded grains with diameter in the range of 340–580 nm were obtained.<sup>38</sup> Spray pyrolysis had also been used to synthesize  $\text{Co}_3\text{O}_4$  and got some overgrown clusters with the average size of 80 nm.<sup>27</sup> Compared to these large grains,  $\text{CoO}_x$  with much smaller grain size was obtained in the present work. Moreover, the tiny structure and loose spatial organization which always accompanied with a high specific surface area are expected to be beneficial to the catalytic performances.

### Chemical composition

To explore the chemical composition of the prepared thin films on stainless steel, XPS was carried out on both bare and etched surfaces of the  $\text{CoO}_x$  films. As depicted in Fig. 4, on the bare surfaces, much carbon was detected, which may be contamination products originated from precursor decomposition and ambient air. After 50 nm etching, carbon contamination is negligible. Fig. 5 and 6 are the Co 2p and O 1s spectra after etching, respectively. To avoid Auger correction effect, only the Co 2p<sub>1/2</sub> spectra were fitted. According to Gautier *et al.*,<sup>39</sup> the Co 2p<sub>1/2</sub> peaks at around 795.0 eV are composed of  $\text{Co}^{2+}$  (796.4 eV) and  $\text{Co}^{3+}$  (795.2 eV). As shown in Fig. 5, all the samples are composed of  $\text{Co}^{2+}$  and  $\text{Co}^{3+}$ . The fitted results are in Table 1,

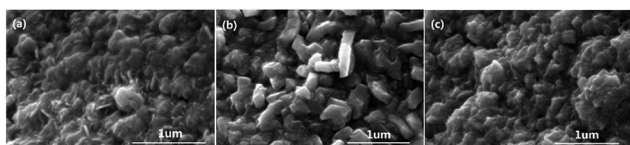


Fig. 3 SEM images of  $\text{CoO}_x$  thin films coated on stainless steel mesh: (a) Mesh 350, (b) Mesh 400 and (c) Mesh 450.

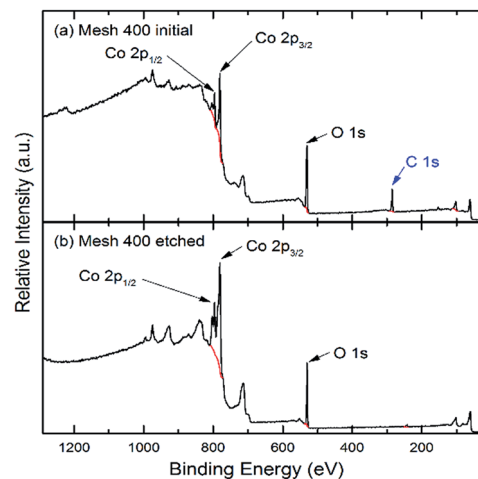


Fig. 4 Entire XPS spectra of Mesh 400 before (a) and after etching (b).

Mesh 350 contains 91% of  $\text{Co}^{2+}$  and the calculated formula is  $\text{CoO}_{1.05}$  which indicates that the main composition of Mesh 350 is  $\text{CoO}$ . Mesh 400 has a similar amount of  $\text{Co}^{2+}$  and  $\text{Co}^{3+}$  and the stoichiometric formula is  $\text{CoO}_{1.29}$ . For Mesh 450, the ratio of Co/O is 3 : 4.11, which is very close to  $\text{Co}_3\text{O}_4$ . These observations further confirm the transformation of  $\text{CoO}$  to pure  $\text{Co}_3\text{O}_4$  as the temperature increases from 350 to 450 °C.

The O 1s spectra of the synthesized films were deconvoluted into two peaks in the binding energy (BE) range of 528–532 eV in Fig. 6. The lower peak is attributed to the lattice oxygen species  $\text{O}^{2-}$ , and the other one is assigned to adsorbed oxygen.<sup>40,41</sup> As depicted in the fitted O 1s spectra, all the samples were composed of two kinds of oxygen. In each sample, the atomic percentage of lattice oxygen was more than 90% and Mesh 400 possesses the most adsorbed oxygen (see Table 1). It is generally recognized that with TMOs catalysts, the lattice oxygen plays an important role in the catalytic oxidation process according to the redox mechanism. However, among the three samples, the amount of lattice oxygen has no much differences. Different amount of adsorbed oxygen may lead to different performances since adsorbed oxygen may create more active sites for catalytic reactions.

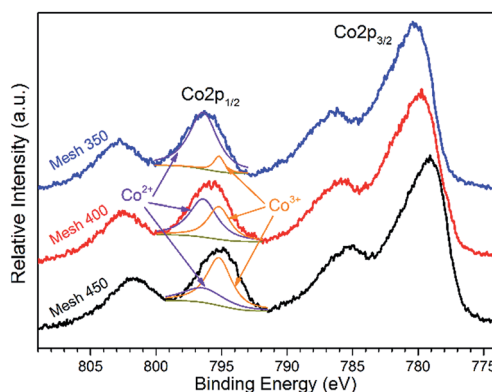


Fig. 5 XPS of Co 2p of the prepared  $\text{CoO}_x$  samples.

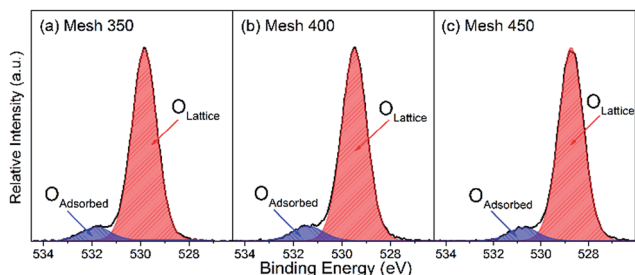


Fig. 6 O 1s signals of  $\text{CoO}_x$  thin films.

Table 1 Results of fitted Co  $2p_{1/2}$  and O 1s of different samples

Sample	Proportion	Stoichiometric formula	Atomic percentage (%)	
	$\text{Co}^{3+} : \text{Co}^{2+}$		$\text{O}_{\text{Lattice}}$	$\text{O}_{\text{Adsorbed}}$
Mesh 350	0.09 : 0.91	$\text{CoO}_{1.05}$	92.1	7.9
Mesh 400	0.58 : 0.42	$\text{CoO}_{1.29}$	91.3	8.7
Mesh 450	0.74 : 0.26	$\text{CoO}_{1.37}$	92.7	7.3

### Catalytic performance

Fig. 7 compares the outlet profiles of  $\text{C}_3\text{H}_6$ , CO and  $\text{C}_2\text{H}_4$  in the oxidation of  $\text{C}_3\text{H}_6$  over three  $\text{CoO}_x$  samples and with NCM as reference. For the three coated meshes, the conversion of  $\text{C}_3\text{H}_6$  becomes measurable at around 200 °C and complete conversion is reached within 400 °C. Mesh 350 and 400 exhibit slight better performance than Mesh 450 for about 25 °C with the complete conversion temperature. For the reaction with NCM, the consumption of  $\text{C}_3\text{H}_6$  was found to be negligible up to 500 °C and 700 °C was needed to attain its complete conversion to  $\text{CO}_2$ . Table 2 summarizes the comparison of the catalytic performance of different catalysts by  $T_{90}$ . It is obvious that  $\text{CoO}_x$  samples prepared in this work are quite competitive to many other TMOs and noble metal catalysts. It is worth mentioning that these catalytic tests were repeated three times with the same sample and the results have no apparent difference (see ESI Fig. S1†), demonstrating that the prepared  $\text{CoO}_x$  has good reusability.

The investigation of  $\text{C}_3\text{H}_6$  oxidation over NCM showed no significant difference compared with a blank system (see ESI Fig. S2†), suggesting that the mesh has a negligible catalytic effect and can be used as an inert carrier for the objective evaluation of deposited catalyst. In each case,  $\text{CO}_2$  was observed to be the final product. CO and  $\text{C}_2\text{H}_4$  were detected during the

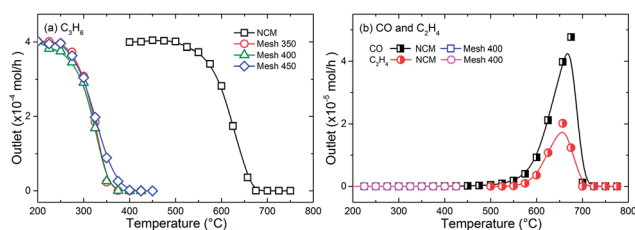


Fig. 7 Outlet profiles of  $\text{C}_3\text{H}_6$  (a), CO and  $\text{C}_2\text{H}_4$  (b).

reaction process over NCM with a considerable amount which can be attributed to the partial oxidation. In contrast, no traces of CO or  $\text{C}_2\text{H}_4$  were detected with any coated meshes, as indicated in Fig. 7b (Mesh 350 and Mesh 450 have overlapped with Mesh 400, so only Mesh 400 was given as a representative), demonstrating that  $\text{CoO}_x$  is an effective catalyst to prevent the formation of CO and  $\text{C}_2\text{H}_4$ .

With an Arrhenius expression for evaluation of the light-off profiles in the region where less than 15% of  $\text{C}_3\text{H}_6$  was converted, apparent activation energies ( $E_{\text{appa}}$ ) were calculated following ref. 17. Fig. 8 compares the  $E_{\text{appa}}$  values obtained in this work. The reaction with Mesh 400 shows relatively low  $E_{\text{appa}}$  ( $78.1 \text{ kJ mol}^{-1}$ ) which indicates its high reactivity at low temperatures. It increases to 107.1 and  $132.6 \text{ kJ mol}^{-1}$  with Mesh 450 and 350, respectively. The non-catalyzed reaction presents an  $E_{\text{appa}}$  of  $95.8 \text{ kJ mol}^{-1}$  which is surprisingly lower than Mesh 350 and 450. Above all,  $E_{\text{appa}}$  is a parameter which focuses only on the initiation of the chemical reactions. Only with a low  $E_{\text{appa}}$  does not mean high-activity and can't promise a low temperature for complete conversion of the fuel molecules. The results indicate that the activity of catalysts increased greatly as temperature increases while NCM exhibits inert activity. For the initiation processes of propene oxidation, crystal defects formed in the preparation of Mesh 350 and 450 samples could make them less active. On the other hand, the oxygen vacant sites, which normally play key roles in the redox mechanism, tend to increase from 350 to 400 °C and then decrease from 400 to 450 °C, enabling Mesh 350 and 450 to exhibit high  $E_{\text{appa}}$  values. This is supported by the lowest  $E_{\text{appa}}$  and best performance for sample Mesh 400. Moreover, the adsorbed oxygen on the NCM could benefit for the initiation of propene oxidation, which leads to a low  $E_{\text{appa}}$  with NCM. Compared with Mesh 350 and Mesh 450, Mesh 400 has a loose spatial organization and so higher specific surface area to absorb more oxygen and fuel, this behavior may promote the activation process. Moreover, from XPS results, Mesh 400 owns the most adsorbed oxygen, which can provide more active sites in the catalytic process. For Mesh 350, though with a higher  $E_{\text{appa}}$ , the complete conversion temperature is lower than Mesh 450 by 25 °C, which can be due to its higher mobility of lattice oxygen according to its better reducibility with more  $\text{Co}^{2+}$ .<sup>42</sup>

### Mechanism

In order to reveal the possible catalytic mechanism over the prepared  $\text{CoO}_x$ , *in situ* DRIFTS was performed. To identify the characteristic peaks of  $\text{C}_3\text{H}_6$ , pure gas of  $\text{C}_3\text{H}_6$  was measured first using an IR chamber and the observed spectrum is showed in ESI Fig. S3.† For this *in situ* DRIFTS test, the spectra with Mesh 400 are presented in Fig. 9 as a representative and the left two spectra of Mesh 350 and 450 could be found in ESI Fig. S4 and S5,† respectively. Fig. 9 depicts the IR spectra at different temperatures. Among these absorption peaks,  $913 \text{ cm}^{-1}$  is assigned to the  $\text{CH}_2$  wagging vibration of adsorbed  $\text{C}_3\text{H}_6$  on the deposited film;<sup>52</sup>  $669 \text{ cm}^{-1}$  comes from the bending vibration of  $\text{CO}_2$ ;  $557$  and  $657 \text{ cm}^{-1}$  are characteristic absorption peaks of  $\text{Co}_3\text{O}_4$  and  $582 \text{ cm}^{-1}$  is attributed to CoO as depicted in Fig. 2.

Table 2 Comparison of  $T_{90}$  of different catalysts

Catalyst	Weight (mg)	Inlet composition	Flow rate (mL min <sup>-1</sup> )	$T_{90}^a$ (°C)	Ref.
Mesh 350	13	1% C <sub>3</sub> H <sub>6</sub> /10% O <sub>2</sub> in Ar	15	347	This work
Mesh 400	13	1% C <sub>3</sub> H <sub>6</sub> /10% O <sub>2</sub> in Ar	15	348	This work
Mesh 450	13	1% C <sub>3</sub> H <sub>6</sub> /10% O <sub>2</sub> in Ar	15	369	This work
Co <sub>3</sub> O <sub>4</sub>	12	1% C <sub>3</sub> H <sub>6</sub> /10% O <sub>2</sub> in Ar	15	380	32
Co <sub>3</sub> O <sub>4</sub>	12	2% C <sub>3</sub> H <sub>6</sub> /20% O <sub>2</sub> in Ar	15	385	43
Co <sub>3</sub> O <sub>4</sub>	41.5	0.4% C <sub>3</sub> H <sub>6</sub> /3.6% O <sub>2</sub> in Ar	500	356	17
Co <sub>2.66</sub> Mn <sub>0.34</sub> O <sub>4</sub>	12	2% C <sub>3</sub> H <sub>6</sub> /20% O <sub>2</sub> in Ar	15	356	43
CuO	12	1% C <sub>3</sub> H <sub>6</sub> /10% O <sub>2</sub> in Ar	15	301	44
Cu <sub>2</sub> O	20	1% C <sub>3</sub> H <sub>6</sub> /10% O <sub>2</sub> in Ar	15	375	45
Mn <sub>3</sub> O <sub>4</sub>	12	1% C <sub>3</sub> H <sub>6</sub> /10% O <sub>2</sub> in Ar	15	403	33
Co <sub>2.1</sub> Fe <sub>0.9</sub> O <sub>4</sub>	20	1% C <sub>3</sub> H <sub>6</sub> /10% O <sub>2</sub> in Ar	15	382	46
CuCo <sub>2</sub> O <sub>4</sub>	12	1% C <sub>3</sub> H <sub>6</sub> /10% O <sub>2</sub> in Ar	15	384	47
La <sub>1.7</sub> Sr <sub>0.3</sub> CuO <sub>4</sub> S <sub>0.2</sub>	200	0.1% C <sub>3</sub> H <sub>6</sub> /5% O <sub>2</sub> in N <sub>2</sub>	100	500	48
Co <sub>0.3</sub> Ce <sub>3</sub> O <sub>6.4</sub>	200	0.1% C <sub>3</sub> H <sub>6</sub> /9% O <sub>2</sub> in He	120	351	49
Au/Al <sub>2</sub> O <sub>3</sub>	4/200	0.15% C <sub>3</sub> H <sub>6</sub> /4% O <sub>2</sub> in He	75	410	50
Au/Al <sub>2</sub> O <sub>3</sub>	8.2/200	0.4% C <sub>3</sub> H <sub>6</sub> /3.6% O <sub>2</sub> in He	30	412	51
NCM	—	1% C <sub>3</sub> H <sub>6</sub> /10% O <sub>2</sub> in Ar	15	648	This work

<sup>a</sup>  $T_{90}$  refers to the temperature at which 90% of the fuel is converted.

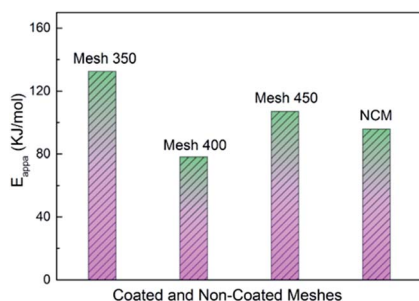


Fig. 8 The apparent activation energy ( $E_{app}$ ) of NCM and coated meshes prepared at 350, 400 and 450 °C during catalytic processes of C<sub>3</sub>H<sub>6</sub>.

As can be seen from Fig. 9, spectra measured below 200 °C had strong adsorption peak of C<sub>3</sub>H<sub>6</sub> (913 cm<sup>-1</sup>). With temperature increasing, adsorption peak of C<sub>3</sub>H<sub>6</sub> vanishes gradually and the peak attribute to CO<sub>2</sub> (669 cm<sup>-1</sup>) become stronger. This indicates that during the catalytic process, C<sub>3</sub>H<sub>6</sub> is adsorbed on the surface of the CoO<sub>x</sub> catalyst firstly, and then the reaction rate of adsorbed C<sub>3</sub>H<sub>6</sub> is accelerated as temperature increases and more CO<sub>2</sub> is generated. With a higher C<sub>3</sub>H<sub>6</sub> consumption rate and so CO<sub>2</sub> production rate, the adsorption peak of C<sub>3</sub>H<sub>6</sub> becomes weaker and the peak of CO<sub>2</sub> becomes stronger. With *in situ* DRIFTS spectra, adsorption of C<sub>3</sub>H<sub>6</sub> on CoO<sub>x</sub> thin films was observed, which suggests that the catalytic reaction of C<sub>3</sub>H<sub>6</sub> on CoO<sub>x</sub> is preceded with the Langmuir–Hinshelwood (L–H) mechanism.

Normally, redox mechanism is accepted for the catalytic oxidation of light hydrocarbons over TMOs as the metal ions can be circulated by reduction to lower ionic states and recovery to higher ionic states *via* re-oxidization.<sup>53–55</sup> In this work, Co<sup>3+</sup> and Co<sup>2+</sup> in the CoO<sub>x</sub> thin films could be reduced to Co<sup>2+</sup> and Co by releasing active oxygen. As temperature increases, adsorbed C<sub>3</sub>H<sub>6</sub> will react with trapped or released oxygen. Co<sup>2+</sup>

and Co can then be reoxidized to form CoO<sub>x</sub> by the replenished oxygen in the gas phase.<sup>56,57</sup> Moreover, the electrophilic oxidation involving chemisorbed species O<sub>2</sub><sup>-</sup> and O<sup>-</sup> will promote the total oxidation of C<sub>3</sub>H<sub>6</sub> to CO<sub>2</sub> over Co<sub>3</sub>O<sub>4</sub>.<sup>57</sup> It's worth noting that the catalysts take part in the reaction during the propene oxidation process and the chemical composition of the active surface is always changing as a consequence of sustainable oxidation–reduction, but the compositions of the catalysts would keep the same before and after the catalytic reaction.<sup>43</sup> This phenomena were also confirmed by running the catalytic tests several times and the same results were obtained. As displayed in Fig. 9, with temperature increased from 50 to 400 °C, the three CoO<sub>x</sub> adsorption bands at 657, 582 and 557 cm<sup>-1</sup> exhibit red shift of 11, 9 and 13 cm<sup>-1</sup>, respectively. The red shift is due to the change of vibration energy level as the temperature increases, which further indicates that more bulk oxygen is

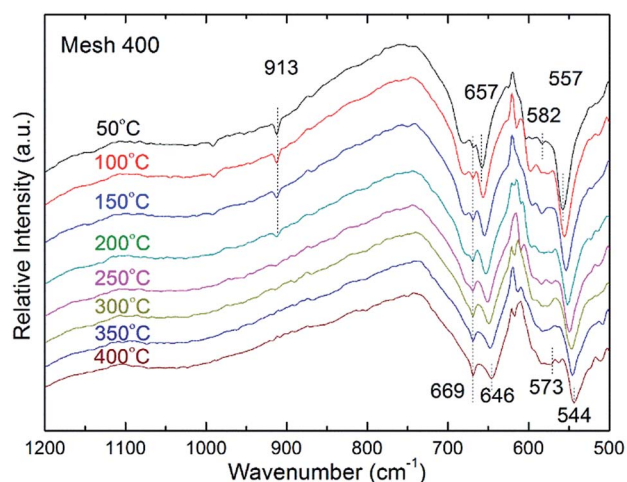


Fig. 9 *In situ* DRIFTS spectra of CoO<sub>x</sub> prepared at 400 °C during C<sub>3</sub>H<sub>6</sub> oxidation at different temperatures.

activated. From the random changes of the relative intensity of CoO and Co<sub>3</sub>O<sub>4</sub>, a sustainable transformation process between Co<sup>3+</sup> and Co<sup>2+</sup> can be proposed, which supports the redox mechanism in the oxidation of C<sub>3</sub>H<sub>6</sub> over CoO<sub>x</sub>.

## Experimental

### Synthesis of CoO<sub>x</sub> films

The CoO<sub>x</sub> thin films were synthesized in a PSE-CVD system combined with cold-wall stagnation point-flow CVD reactor and waste collector. The experimental setup can be found in our previous work<sup>45</sup> and typical deposition conditions are shown in ESI Table S1,† respectively. Cobalt acetylacetonate (Co(acac)<sub>2</sub>) was dissolved in ethanol with a concentration of 2.5 mM as the feedstock. The frequency and width of the injector are 4 Hz and 1.2 ms. The liquid feedstock, with a feeding rate of 1.0 mL min<sup>-1</sup>, was injected as a fine spray into a 30 cm long evaporation chamber kept at 220 °C. The resulting vapor was transported to the deposition chamber, with N<sub>2</sub>/O<sub>2</sub> flow rates of 0.25/0.75 standard liter per minute (SLM), respectively. Flow rates of gases were controlled by MKS mass flow controllers. The total pressure in the reactor during deposition was kept at 3.0 kPa. To meet the requirements of different characterization techniques, the deposition was performed on several types of substrates without any treatments, including bare glass, stainless steel and mesh grid of stainless steel. Mesh 350, Mesh 400 and Mesh 450 are defined as the deposited films on relevant substrate at 350, 400 and 450 °C, respectively. The substrates were heated using a flat resistive heater by a heating controller (HT60, Horst). The waste vapor was collected by a liquid nitrogen trap and the rest gases were pumped away. The weight of the deposited films was determined gravimetrically by measuring the weight change of the substrates with a microbalance (Sartorius).

### Characterization

The phases of the deposited films obtained at different substrate temperatures were identified by X-ray diffraction (XRD) using a Bruker D8 Focus equipped with a Cu K $\alpha$  ( $\lambda = 0.154056$  nm) radiation source and operated at 40 kV and 40 mA. By referring to the Joint Committee on Powder Diffraction Standards (JCPDS) database cards, the crystalline phases were identified. The morphology of the deposited films was examined using SEM (QUANTA FEG 250). The characteristic vibrations of the prepared thin film catalysts were ascertained using a diffuse reflectance infrared Fourier transform spectroscopy (DRIFTS, Bruker VERTEX 70) with the spectral resolution of 4 cm<sup>-1</sup> in the range of 400–4000 cm<sup>-1</sup>.

### Catalytic test

Small unsaturated hydrocarbons, such as propene (C<sub>3</sub>H<sub>6</sub>), is an important class of VOCs and quite difficult to be oxidized. In this work, the catalytic behavior of CoO<sub>x</sub> was investigated toward the oxidation of C<sub>3</sub>H<sub>6</sub> at atmospheric pressure in a fixed-bed quartz reactor with 13 mg catalyst grown on meshes of stainless steel. To exclude the effect of background, a contrast test using mesh grid without any deposition was performed. The experimental

setup can be found elsewhere<sup>45</sup> and only a brief description is given here. A feed mixture of 1 vol% C<sub>3</sub>H<sub>6</sub> and 10 vol% O<sub>2</sub> in the balance of argon was introduced into a tubular reactor at a total flow rate of 15 mL min<sup>-1</sup>, corresponding to weight hourly space velocity (WHSV) of about 69 000 mL g<sub>cat</sub><sup>-1</sup> h<sup>-1</sup>. The temperature of the reactor was raised with a ramp of 5 °C min<sup>-1</sup> using a digital electrical furnace. The exhaust gases were analyzed using a gas chromatograph (Agilent, GC3000).

To explore the catalytic mechanism, *in situ* DRIFTS tests were carried out. The stainless steel mesh with deposition was placed in the temperature-controlled chamber. C<sub>3</sub>H<sub>6</sub>/O<sub>2</sub>/Ar with the ratio of 1%/10%/89% and a total flow rate of 15 mL min<sup>-1</sup> were introduced into the chamber. The temperature of the chamber was raised with a ramp of 5 °C min<sup>-1</sup> from room temperature to 400 °C during the tests. The background spectrum was deducted by measuring the spectrum of a non-coated mesh (NCM) in the *in situ* chamber under the same gas inlet conditions. By online monitoring the transform of the characteristic bands of CoO<sub>x</sub> and absorption of fuel gases, possible catalytic mechanism can be proposed.

## Conclusions

The one-step PSE-CVD method was applied to prepare CoO<sub>x</sub> thin films from Co(acac)<sub>2</sub> by adjusting the temperature from 350 to 450 °C. The obtained samples were characterized in terms of structure, morphology, surface composition and catalytic properties with XRD, FTIR, SEM, XPS and *in situ* DRIFTS. Structure studies demonstrate that with an increase of substrate temperature from 350 to 450 °C, the obtained oxides varied from CoO to pure Co<sub>3</sub>O<sub>4</sub> spinel gradually. Adsorption of oxygen species is more with Mesh 400 than 350 and 450 which may benefit the catalytic performances. Catalytic tests indicate that CoO<sub>x</sub> exhibit a competitive catalytic activity compared to supported noble metals and many other TMOs in the deep oxidation of C<sub>3</sub>H<sub>6</sub>. Mesh 350 and 400 showed slightly better performance over Mesh 450 due to its more low-valence cobalt, porous structure and more adsorbed oxygen. With increasing temperature, adsorption peaks of C<sub>3</sub>H<sub>6</sub> and CO<sub>2</sub> were detected and surface conversion of CoO–Co<sub>3</sub>O<sub>4</sub> was also observed during *in situ* DRIFTS tests. These observations indicate that the catalytic reaction was preceded with redox and L–H mechanism.

## Acknowledgements

ZYT thanks the financial support from the Recruitment Program of Global Youth Experts. The authors thank Dr Jun-Jie Weng and Mr Bing-Yin Wang for help discussions.

## Notes and references

- 1 J. J. Schauer, M. J. Kleeman, G. R. Cass and B. R. T. Simoneit, *Environ. Sci. Technol.*, 2001, **35**, 1716–1728.
- 2 C. J. Cai, F. H. Geng, X. X. Tie, Q. O. Yu and J. L. An, *Atmos. Environ.*, 2010, **44**, 5005–5014.
- 3 P. R. Veres, P. Faber, F. Drewnick, J. Lelieveld and J. Williams, *Atmos. Environ.*, 2013, **77**, 1052–1059.

- 4 S. Batterman, F. C. Su, S. Li, B. Mukherjee, C. R. Jia and H. E. I. H. R. Committee, *Res. Rep.-Health Eff. Inst.*, 2014, 3–63.
- 5 T. Y. Chang and M. J. Suzio, *J. Air Waste Manage. Assoc.*, 1995, 45, 20–28.
- 6 US, EPA, *Air pollution control technology fact sheet*, EPA-452/F-03-022.
- 7 G. Chen, K. A. Strevett and B. A. Vanegas, *Biodegradation*, 2001, 12, 433–442.
- 8 W. J. Cooper, M. G. Nickelsen, R. V. Green and S. P. Mezyk, *Radiat. Phys. Chem.*, 2002, 65, 571–577.
- 9 A. M. Mastral, T. Garcia, M. S. Callén, J. M. López, M. V. Navarro, R. Murillo and J. Galbán, *Environ. Sci. Technol.*, 2002, 36, 1821–1826.
- 10 H. L. Huang and W. M. Lee, *J. Environ. Eng.*, 2002, 128, 60–67.
- 11 E. N. Ndifor, T. Garcia, B. Solsona and S. H. Taylor, *Appl. Catal., B*, 2007, 76, 248–256.
- 12 K. Everaert and J. Baeyens, *J. Hazard. Mater.*, 2004, 109, 113–139.
- 13 P. Papaefthimiou, T. Ioannides and X. E. Verykios, *Appl. Catal., B*, 1997, 13, 175–184.
- 14 S. Minicò, S. Scirè, C. Crisafulli, R. Maggiore and S. Galvagno, *Appl. Catal., B*, 2000, 28, 245–251.
- 15 Z. Gu and K. L. Hohn, *Ind. Eng. Chem. Res.*, 2004, 43, 30–35.
- 16 L. F. Liotta, M. Ousmane, G. Di Carlo, G. Pantaleo, G. Deganello, A. Boreave and A. Giroir-Fendler, *Catal. Lett.*, 2009, 127, 270–276.
- 17 Z. Y. Tian, N. Bahlawane, F. Qi and K. Kohse-Höinghaus, *Catal. Commun.*, 2009, 11, 118–122.
- 18 R. Edla, N. Patel, Z. El Koura, R. Fernandes, N. Bazzanella and A. Miotello, *Appl. Surf. Sci.*, 2014, 302, 105–108.
- 19 K. Shojaee, B. S. Haynes and A. Montoya, *Appl. Surf. Sci.*, 2014, 316, 355–365.
- 20 Z. Y. Tian, N. Bahlawane, V. Vannier and K. Kohse-Höinghaus, *Proc. Combust. Inst.*, 2013, 34, 2261–2268.
- 21 A. Goyal, S. Bansal, V. Kumar, J. Singh and S. Singhal, *Appl. Surf. Sci.*, 2015, 324, 877–889.
- 22 A. Jamal, M. M. Rahman, S. B. Khan, M. Faisal, K. Akhtar, M. A. Rub, A. M. Asiri and A. O. Al-Youbi, *Appl. Surf. Sci.*, 2012, 261, 52–58.
- 23 D. H. Shang, Q. Zhong and W. Cai, *Appl. Surf. Sci.*, 2015, 325, 211–216.
- 24 K. J. Kim and Y. R. Park, *Solid State Commun.*, 2003, 127, 25–28.
- 25 P. S. Patil, L. D. Kadam and C. D. Lokhande, *Thin Solid Films*, 1996, 272, 29–32.
- 26 H. Yamamoto, S. Tanaka and K. Hirao, *J. Appl. Phys.*, 2003, 93, 4158–4162.
- 27 V. R. Shinde, S. B. Mahadik, T. P. Gujar and C. D. Lokhande, *Appl. Surf. Sci.*, 2006, 252, 7487–7492.
- 28 H. Heli and H. Yadegari, *Electrochim. Acta*, 2010, 55, 2139–2148.
- 29 L. Poul, S. Ammar, N. Jouini, F. Fiévet and F. Villain, *Solid State Sci.*, 2001, 3, 31–42.
- 30 K. Deori and S. Deka, *CrystEngComm*, 2013, 15, 8465–8474.
- 31 G. L. Zhou, H. M. Xie, B. G. Gui, G. Z. Zhang and X. X. Zheng, *Catal. Commun.*, 2012, 19, 42–45.
- 32 P. Mountapmbeme Kouotou, Z. Y. Tian, U. Mundloch, N. Bahlawane and K. Kohse-Höinghaus, *RSC Adv.*, 2012, 2, 10809–10812.
- 33 Z. Y. Tian, P. Mountapmbeme Kouotou, N. Bahlawane and P. H. Tchoua Ngamou, *J. Phys. Chem. C*, 2013, 117, 6218–6224.
- 34 N. Bahlawane, P. H. Tchoua Ngamou, V. Vannier, T. Kottke, J. Heberle and K. Kohse-Höinghaus, *Phys. Chem. Chem. Phys.*, 2009, 11, 9224–9232.
- 35 V. Vannier, M. Schenk, K. Kohse-Höinghaus and N. Bahlawane, *J. Mater. Sci.*, 2012, 47, 1348–1353.
- 36 M. Lenglet, J. Lopitiaux, L. Terrier, P. Chartier, J. F. Koenig, E. Nkeng and G. Poillerat, *J. Phys. IV*, 1993, 3, 477–483.
- 37 B. Lefez, P. Nkeng, J. Lopitiaux and G. Poillerat, *Mater. Res. Bull.*, 1996, 31, 1263–1267.
- 38 D. Barreca, C. Massignan, S. Daolio, M. Fabrizio, C. Piccirillo, L. Armelao and E. Tondello, *Chem. Mater.*, 2001, 13, 588–593.
- 39 J. L. Gautier, E. Rios, M. Gracia, J. F. Marco and J. R. Gancedo, *Thin Solid Films*, 1997, 311, 51–57.
- 40 G. Tyuliev and S. Angelov, *Appl. Surf. Sci.*, 1988, 32, 381–391.
- 41 S. Valeri, A. Borghi, G. C. Gazzadi and A. di Bona, *Surf. Sci.*, 1999, 423, 346–356.
- 42 P. Mountapmbeme Kouotou, Z. Y. Tian, H. Vieker, A. Beyer, A. Golzhauser and K. Kohse-Höinghaus, *J. Mater. Chem. A*, 2013, 1, 10495–10504.
- 43 Z. Y. Tian, P. H. Tchoua Ngamou, V. Vannier, K. Kohse-Höinghaus and N. Bahlawane, *Appl. Catal., B*, 2012, 117–118, 125–134.
- 44 Z. Y. Tian, H. J. Herrenbrück, P. Mountapmbeme Kouotou, H. Vieker, A. Beyer, A. Gözlhäuser and K. Kohse-Höinghaus, *Surf. Coat. Technol.*, 2013, 230, 33–38.
- 45 G. F. Pan, S. B. Fan, J. Liang, Y. X. Liu and Z. Y. Tian, *RSC Adv.*, 2015, 5, 42477–42481.
- 46 Z. Y. Tian, P. Mountapmbeme Kouotou, A. El Kasmi, P. H. Tchoua Ngamou, K. Kohse-Höinghaus, H. Vieker, A. Beyer and A. Gözlhäuser, *Proc. Combust. Inst.*, 2015, 35, 2207–2214.
- 47 Z. Y. Tian, H. Vieker, P. Mountapmbeme Kouotou and A. Beyer, *Faraday Discuss.*, 2015, 177, 249–262.
- 48 M. Machida, K.-i. Ochiai, K. Ito and K. Ikeue, *J. Catal.*, 2006, 238, 58–66.
- 49 L. F. Liotta, M. Ousmane, G. Di Carlo, G. Pantaleo, G. Deganello, G. Marci, L. Retailleau and A. Giroir-Fendler, *Appl. Catal., A*, 2008, 347, 81–88.
- 50 S. Ivanova, C. Petit and V. Pitchon, *Gold Bull.*, 2006, 39, 3–8.
- 51 A. C. Gluhoi, N. Bogdanchikova and B. E. Nieuwenhuys, *J. Catal.*, 2005, 229, 154–162.
- 52 P. R. Griffiths and J. A. de Haseth, *Fourier transform infrared spectrometry*, John Wiley & Sons, 2007.
- 53 M. Labanowska, *ChemPhysChem*, 2001, 2, 712–731.
- 54 I. Aso, M. Nakao, N. Yamazoe and T. Seiyama, *J. Catal.*, 1979, 57, 287–295.
- 55 M. Konsolakis, M. Sgourakis and S. A. Carabineiro, *Appl. Surf. Sci.*, 2015, 341, 48–54.
- 56 D. Duprez, *Catal. Today*, 2006, 112, 17–22.
- 57 J. Haber and W. Turek, *J. Catal.*, 2000, 190, 320–326.